VICTORIA UNIVERSITY
MELBOURNE AUSTRALIA

Towards a quantitative indicator of feather disruption following the cleansing of oiled birds

This is the Accepted version of the following publication

The publisher's official version can be found at
https://www.ncbi.nlm.nih.gov/pubmed/28526197
Note that access to this version may require subscription.

Towards a quantitative indicator of feather disruption following the cleansing of oiled birds

Stephen W. Bigger[1]*, Lawrence N. Ngeh[1], Peter Dann[2] and John D. Orbell[1]

1. Institute for Sustainability and Innovation, College of Engineering and Science, Victoria University, PO Box 14428, Melbourne, 8001, Australia.
2. Research Department, Phillip Island Nature Parks, PO Box 97, Cowes, Phillip Island, 3991, Australia.

R E V I S E D   M A N U S C R I P T

Abstract

A computer-based imaging method for determining feather microstructure coherency following a cleansing treatment, was developed, calibrated and trialled on Mallard Duck (*Anas platyrhyhchos*) feathers. The feathers were initially contaminated with a light crude oil and then cleansed by either detergent (Deacon 90) treatment or, alternatively, by magnetic particle technology (MPT) using iron powder. The imaging method provides a single quantitative parameter for the coherence of feather microstructure and the results confirm that MPT treatment imparts less disruption to the feather microstructure than detergent treatment. It is proposed that this imaging method can be developed and implemented for the assessment of feather disruption and possibly damage, either for the trialling of different treatment protocols, or as a tool during the rehabilitation process, along with other such indicators, to give a more comprehensive assessment of feather condition than is currently available.

Key Words

Computer-imaging; feather microstructure coherency; magnetic particle cleansing; oil-soaked birds

Highlights

- Computer-based imaging method developed to quantitatively assess feather coherency.
- Imaging method successfully applied in studying cleansing of oil-soaked feathers and to feather coherency assessment.
- Cleansing feathers magnetically imparts less disruption to feather integrity than detergent methods.

*Author for correspondence

48   **1. Introduction**
49
50   Magnetic particle technology (MPT) has demonstrated great utility in a range of
51   discipline areas (Safarikova & Safarik, 2001) and is a convenient and quick means by
52   which oil-soaked wildlife can be cleansed (Orbell *et al*., 2007). This innovative
53   approach has been investigated and developed for the clean-up of oil-soaked species
54   such as the Mallard Duck (*Anas platyrhynchos*) and Little Penguin (*Eudyptula minor*)
55   (Orbell *et al*., 2004). This technology has the advantage of being portable and enables
56   oil to be removed immediately in the field, upon first encounter, either directly or with
57   the aid of pre-treatment agents in cases where the oil residues are highly weathered
58   and/or persistent (Ngeh *et al*., 2012).
59
60   Two further advantages of MPT technology over detergent-based techniques for oil
61   removal are its high efficiency and its purported ability to invoke less damage to the
62   feather microstructure (Orbell *et al*., 2007). In relation to exploring the removal
63   efficiency of MPT it has been necessary to develop a quantitative assay (Orbell *et al.*,
64   1997) that can be used to compare the efficiency of MPT technology with those
65   efficiencies offered by detergent cleansing. To this end, computer-assisted analyses
66   such as those developed for the sequestering (Bigger *et al.*, 2010) and the sequential
67   pick-up (Bigger *et al.*, 2013) of chemical contaminants by MPT have been used to
68   process gravimetric laboratory data to quantitatively and objectively determine the
69   efficiency of oil removal under a variety of conditions.
70
71   The quantitative assessment of feather condition as indicated by its coherency, on the
72   other hand, remains an area still to be developed. It has long been recognized that
73   feather condition, as manifested in the ability of feathers to repel water, is a key factor
74   governing the decision as to when to release a rehabilitated bird back into the wild
75   (Ngeh, 2002). Work on the quantitative assessment of feather condition includes
76   early studies that applied a theory of water repellence developed by Cassie and Baxter
77   (1944) for woven fabrics and textiles, to the structure of a feather vane (Rijke, 1968;
78   Rijke, 1970; Rijke *et al*., 2000). It was proposed that the water repellence of contour
79   feathers is mathematically related to the radius of the feather barb and the half-
80   distance between the axes of the barb (Stephenson, 1997; Stephenson & Andrews,
81   1997).
82
83   Further to these early studies, there appears to be very little available literature on the
84   quantitative assessment of feather condition following, say, cleansing or other
85   rehabilitation treatments. Those that have been reported and that provide a
86   quantitative, or at least semi-quantitative, assessment of feather condition, have been
87   developed to varying extents. For example, the presence of preening oils in feathers
88   has long been recognized as an important factor in enabling the feather to repel water
89   (Elder, 1954; Stettenheim, 1972; Elowson, 1984). Based on this observation, the use
90   of gas chromatography to quantify levels of preening oils and waxes in feathers taken
91   from rehabilitating birds has been explored as a possible method leading to the

92   assessment of feather condition (Murray, 1962; Odham & Stenhagen, 1971). Other
93   studies on the assessment of feather condition include those that report the semi-
94   quantitative assessment of wing feather mite infestations on songbirds (Behnke *et al*.,
95   1999; Carleton & Proctor, 2010) and the use of infrared thermography to assess laying
96   hen feather coverage (Zhao *et al*., 2013).
97
98   A notable and more recent contribution is the work of O'Hara and Morandin (2010)
99   who developed a barbule amalgamation index that is calculated from measurements
100   made of feather rami taken from micrograph images. This index was used as an
101   indicator of feather condition following exposure to oil sheens. A quantitative
102   assessment such as this can be of significant value in the overall assessment of the
103   condition of a bird such as a Little Penguin and, hence, in determining when to release
104   it from a rehabilitation facility. To date, the standard international practice for
105   deciding on the water repellency of the plumage has been to place the penguin in a
106   pool at various stages in the rehabilitation process, monitor its behaviour and
107   buoyancy, inspect the degree of water penetration into the plumage, and make a
108   subjective assessment accordingly (Stocker, 2000; Department of Primary Industries,
109   2012). Clearly, to have a high rehabilitation success rate such practice requires a high
110   level of experience and expertise in judging when the bird's plumage is fully water-
111   proof and ready for release.
112
113   In view of the need for the further development of quantitative methods for the
114   assessment of feather condition, this paper describes a computer-assisted imaging
115   method that can be used to provide a quantitative indication of feather microstucture
116   coherency following treatment by detergent or other cleansing actions. It is proposed
117   that the coherence of the feather structure is an important factor that should be
118   considered along with other factors such as the levels of preening oils and waxes
119   when considering the water resistance and thermal insulating properties of the feather.
120   As such, the coherence of the feather structure can be explored as an important
121   indicator of feather condition. An indicator such as this may also have potential
122   future use in a range of veterinary and husbandry applications.
123
124   **2. Methods**
125
126   2.1 Materials and Feather Characterization
127
128   Samples of breast feathers of the Mallard Duck (*Anas platyrhyhchos*) were used in
129   this study[1]. These feathers were initially contaminated with a light crude oil (Esso,
130   Australia, Ltd.; viscosity 11.4 cP) by immersion in the oil for 1 min. Randomly
131   selected and uncontaminated duck feathers were used as a control. A 5% (v/v)

---

[1] The breast feathers of the Mallard Duck are ideal for this *proof of principle* study since they have a well-defined 2-D grid microstructure (Orbell *et al.,* 1999). It is appreciated, however, that feather microstructure is highly variable from one species to another and a specific microstructure parameter would need to be developed for each individual feather type.

132   cleansing detergent solution was prepared by mixing 10 mL of Decon 90™ with 190

133   mL of distilled water. Iron particles having an average maximum dimension of 0.21

134   mm were obtained from Hoganas, Sweden (grade C100.29). The particles were

135   removed from the feathers using a "laboratory magnetic tester" supplied by Alpha

136   Magnetics, Victoria, Australia (Orbell *et al.*, 1997).

137

138   <u>2.2 Feather Treatment and Optical Microscopy</u>

139

140   The detergent cleansing technique involved holding a clustered sample of 5 or 6 oiled

141   feathers by their quills (calami) and agitating in the detergent solution for a period of

142   10 min. The feathers were then rinsed by agitating them in distilled water for 5 min

143   and were left to dry in air for one week. The magnetic particle cleansing treatment

144   involved completely covering a cluster of oiled feathers with the iron particles in a

145   Petri dish and removing all the particles with 1 to 3 continuous sweeps of the

146   laboratory magnetic tester.

147

148   Treated single feather samples were placed on a glass plate and clamped on the stage

149   of a Nikon optical microscope (Labophot Model 248625). Micrographs of the

150   samples were obtained using Nikon Model 401 SLR camera fitted to the microscope.

151

152   <u>2.3 Grid-Generating Algorithm</u>

153

154   A Monte Carlo computer program was written to calculate the area distribution

155   histogram of the quadrilateral elements in a randomly disrupted two-dimensional grid

156   as a function of the extent of the imposed disruption to the grid. In the program, a

157   square grid of side dimensions, S, comprising $n \times n$ elements was generated as a series

158   of $n + 1$ horizontal and vertical intervals drawn between the sets of points P_1 and P_2

159   whose coordinates are: $P_{H,1}[x_H(i, 1), y_H(i, 1)]$; $P_{H,2}[x_H(i, 2), y_H(i, 2)]$; $P_{V,1}[x_V(i, 1)$,

160    $y_V(i, 1)]$ and $P_{V,2}[x_V(i, 2), y_V(i, 2)]$ and where $1 \leq i \leq n + 1$. The subscripts H and V

161   represent the horizontal and vertical components respectively. The allowed

162   deviations of the termini of each interval from their original positions on the grid is

163   given by:

164

165        $d = f \times S/(2n)$ (1)

166

167   where $0 < f < 1$. The parameter, f, is a constant that is set before the program is run

168   and controls the extent of random disruption to the grid. The horizontal and vertical

169   intervals within the perimeter of the square S are randomly disrupted by resetting the

170   coordinates of their termini to: $P_{H,1}[0, i \times S/n + k \times d]$; $P_{H,2}[S, i \times S/n + k \times d]$; $P_{V,1}[i$

171    $\times S/n + k \times d, 0)]$ and $P_{V,2}[i \times S/n + k \times d, S]$, where $2 \leq i \leq n$ and the constant, k, is

172   generated randomly by the computer and lies within the limits $0 \leq k \leq 1$. The sign of

173   k is also generated randomly by the computer.

174 A matrix of intercepts $\{x_{\text{int}}(i, j), y_{\text{int}}(i, j)\}$ is generated for the intersection of each pair

175 of intervals for $\{(i, j): 2 \leq (i, j) \leq n\}$ using the following system of linear equations:

176

177 $$d_1 = x_{\text{H}}(i, 2) - x_{\text{H}}(i, 1) \tag{2}$$

178

179 $$m_1 = [y_{\text{H}}(i, 2) - y_{\text{H}}(i, 1)]/d_1, \text{ for } d_1 \neq 0 \tag{3}$$

180

181 $$d_2 = x_{\text{V}}(j, 2) - x_{\text{V}}(j, 1) \tag{4}$$

182

183 $$m_2 = [y_{\text{V}}(j, 2) - y_{\text{V}}(j, 1)]/d_2, \text{ for } d_2 \neq 0 \tag{5}$$

184

185 $$d_3 = m_2 - m_1 \tag{6}$$

186

187 $$x_{\text{int}}(i, j) = [m_2 x_{\text{V}}(j, 1) - m_1 x_{\text{H}}(i, 1) + y_{\text{H}}(i, 1) - y_{\text{V}}(j, 1)]/d_3, \text{ for } d_3 \neq 0 \tag{7}$$

188

189 $$y_{\text{int}}(i, j) = m_1[x_{\text{int}}(i, j) - x_{\text{H}}(i, 1)] + y_{\text{H}}(i, 1) \tag{8}$$

190

191 The area, A, of a quadrilateral $Q(P_1, P_2, P_3, P_4)$ defined by the points $P_1(x_1, y_1)$,

192 $P_2(x_2, y_2)$, $P_3(x_3, y_3)$, and $P_4(x_4, y_4)$ is given by equation (9) if P_1, P_2, P_3 and P_4 lie in

193 sequential order on the perimeter (McLanaghan & Levy, 1996):

194

195 $$A = [(x_1 y_2 - x_2 y_1) + (x_2 y_3 - x_3 y_2) + (x_3 y_4 - x_4 y_3) + (x_4 y_1 - x_1 y_4)]/2 \tag{9}$$

196

197 The area of each quadrilateral in the randomly disrupted grid is calculated

198 systematically from the matrix of intercepts (see equations (7) and (8)) and stored in

199 the array $A(i)$ where $1 < i < n^2$. The array $A(i)$ is then used to generate a frequency-

200 area histogram upon multiple Monte Carlo iterations of the above algorithm.

201

202 2.4 Image Analysis Algorithm

203

204 Optical micrographs of feather images in the form of black and white photographic

205 jpeg files were analysed using an imaging algorithm designed to systematically count

206 white pixel areas and compile a frequency-area (count) histogram. The jpeg

207 photographic standard stores images as a two-dimensional array of pixel information,

208 each pixel having a red, blue and green (R, B, G) component along with "alpha"

209 channel information associated with each pixel that determines its transparency.

210

211 The devised image processing algorithm firstly removes grey-scale shading (where R,

212 G, B values are all equal but not equal to zero) from the image file by systematically

213 examining the R, G, B information associated with each pixel and setting the pixel to

214 either "white" ($R = 255, G = 255, B = 255$) or "black" ($R = 0, G = 0, B = 0$) in

215 accordance with a $(R_{\text{t}}, G_{\text{t}}, B_{\text{t}})$ threshold set by the user. The algorithm then counts the

216 number of sequential white pixels in each line of the image array and compiles a

217   histogram of the frequency of a given number of sequential white pixels. The latter is
218   deemed to be directly related to the distribution of areas appearing within the grid
219   pattern created by the feather microstructure.
220
221   Provision was made in the software to execute averaging cycles on the raw histogram
222   data. In each cycle the average frequency of two successive frequencies in the
223   histogram is calculated and recorded as the frequency of the upper of the two
224   corresponding area ranges. This process has the effect of smoothing the distribution
225   for the convenient analysis of the associated characteristic parameters. For the
226   systems reported in the current work only one data averaging cycle was found to be
227   necessary.
228

229   **3. Results and Discussion**

230

231   <u>3.1 Analysis of Computer-Generated Grids</u>

232

233   Figure 1 shows three grids that were generated by the Monte Carlo computer
234   algorithm using three levels of grid disruption. The different extent of disruption to
235   the coherence of the grid pattern can be clearly seen as the disruption factor, f, is
236   increased from zero to 1.0.

237

238   >>>Insert Figure 1

239

240   The distribution of the individual quadrilateral areas comprising the grid as a function
241   of the degree of disruption of the grid was explored by generating multiple grids at a
242   given extent of disruption (f) and accumulating the frequencies in the area distribution
243   histogram. The areas of the individual quadrilaterals comprising the grid were
244   calculated in accordance with equation (9). The results are shown in Figure 2 for a
245   selection of 20×20 grids generated with various values of the f parameter and where
246   each frequency is the cumulated frequency after 100 iterations of the Monte Carlo
247   grid disruption cycle and where a resolution of 50 area channels was used.

248

249   >>>Insert Figure 2

250

251   It is clear from Figure 2 that the width of the theoretical area distribution increases as
252   the extent of disruption to the grid increases. There is also a noticeable shift in the
253   maximum towards a lower value of the mean area with increasing values of f and
254   possible evidence of a bimodal distribution of the quadrilateral grid areas at the
255   extreme $f = 1$ value. The observation that there is a general broadening of the
256   distribution with increasing f values supports the notion that the width of the area
257   distribution function is an indicator of the extent of disruption to the coherence of the
258   grid. To test the latter notion, the ratio w/h where w is the width of the distribution
259   taken across the distribution at a frequency corresponding to half the maximum
260   frequency, h, was plotted as a function of f. This plot is shown in Figure 3 for the grid

261 generating conditions used to create the data shown in Figure 2 and calculating data
262 for f values ranging from 0.1 to 1.0 at increments of 0.1.
263
264 >>>Insert Figure 3
265
266 The data in Figure 3 suggest that a high degree of correlation exists between the w/h
267 ratio and the extent of disruption to the coherence of the grid. The relationship
268 appears to be non-linear with the sensitivity of the w/h ratio as a measure of grid
269 coherency increasing with an increasing extent of disruption. It is also clear that the
270 distribution of the separate areas that comprise the overall grid can, in principle, be
271 used to measure the overall coherence of the grid pattern.
272
273 <u>3.2 Image Analysis</u>
274
275 3.2.1 Image Analysis of Computer-Generated Grids
276
277 Having established theoretically the relationship between the w/h ratio and the f
278 parameter, images of the computer-generated grids were analysed using the image
279 analysis algorithm to produce area distribution data that could be compared with those
280 data calculated directly from the grid-generating algorithm.
281
282 Figure 4 shows a selection of area distribution plots where the data were obtained by
283 applying the image analysis algorithm to grid images (20×20 grids; 200×200
284 pixels) that were, in turn, generated by the grid-generating algorithm. The histogram
285 data were processed using one averaging cycle.
286
287 >>>Insert Figure 4
288
289 Inspection of Figure 4 reveals similar behaviour to that observed in Figure 2 and
290 suggests that the image analysis algorithm may be used to determine area distribution
291 data from a micrograph image and subsequently the w/h ratio for these data. To
292 explore this further a series of images of computer-generated grids with values of the f
293 parameter ranging from 0.1 to 1.0 at increments of 0.1 was processed using the image
294 analysis algorithm and the w/h ratio for each grid was determined. Figure 5 shows a
295 plot of the w/h ratio as a function of the f parameter.
296
297 >>>Insert Figure 5
298
299 Figure 5 reveals a high degree of correlation between the two variables, as was also
300 observed in the case of Figure 3, and the relationship between the two variables is,
301 once again, non-linear. The correspondence between the pixel areas as determined by
302 the image analysis algorithm (i.e. a linear pixel-counting routine) and the actual areas
303 of the grid quadrilaterals (i.e. calculated in accordance with equation (9)) can be
304 confirmed by plotting the corresponding w/h ratios derived from each of these

305   techniques for the same series of computer-generated disrupted grids. Such a plot is

306   presented in Figure 6 where $(w/h)_{\text{img anal}}$ is the *w/h* ratio determined from the image

307   analysis algorithm and $(w/h)_{\text{calc}}$ is the *w/h* ratio determined by calculation in

308   accordance with equation (9).

309

310   >>>Insert Figure 6

311

312   The linearity of the plot in Figure 6 confirms that the image analysis algorithm

313   produces a reliable representation of the area distribution histogram of a disrupted

314   two-dimensional grid and can therefore be explored further for use in determining the

315   *w/h* ratio in the case of a feather micrograph image.

316

317   3.2.2 Benchmarking Image Analysis Algorithm

318

319   Previous preliminary work on feather image analysis (Ryan, 2005; Ngeh, 2002)

320   calibrated the area distributions of feather grid patterns that were determined utilizing

321   software that was commercially available at the time (Ryan, 2005) against

322   distributions that were determined from a manual "cut and weigh" (CW) method. The

323   latter involved carefully cutting out the individual grid elements from an enlarged

324   print of the micrograph of the feather and weighing the individual pieces to indirectly

325   determine the separate areas (Ryan, 2005). These data were then used to compile the

326   area distribution histogram. The CW method is clearly quite tedious and can be

327   considered somewhat subjective in that it can be difficult to treat consistently the

328   "grey scale" regions of the image. Nonetheless, the method does provide a reasonable

329   benchmark distribution to test the image analysis algorithm and from which to make

330   meaningful comparisons. Furthermore, the method can overcome a difficulty that

331   was experienced when using the commercially available area imaging software where

332   the software did not always distinguish correctly each of the individual area

333   components comprising the grid-like pattern. It is therefore suggested that the pixel

334   counting algorithm described in the current work can provide a more reliable and

335   consistent analysis of the image as it systematically counts every sequence of white

336   pixels in the image and, as such, does not rely on the correct initial identification of

337   the separate area boundaries.

338

339   The image analysis algorithm was further tested on the image of a feather that was

340   previously characterized (Ryan, 2005) using the CW method described above. Figure

341   7 shows the area distribution histograms of the grid of a duck feather sample where

342   the respective histograms were independently obtained using the image analysis

343   algorithm (158 × 290-pixel micrograph) and the CW method.

344

345   >>>Insert Figure 7

346

347   To directly compare the two histograms, both the frequency and area domains were
348   normalized with the frequency domain being normalized at the maximum frequency.
349   Each distribution was fitted with a 6th order polynomial function to subsequently
350   achieve a consistent analysis of its characteristic w/h parameter. Moreover, Figure 7
351   shows a satisfactory extent of superposition of the two distributions and further
352   analyses of these reveals a w/h ratio calculated *via* the data obtained from the image
353   analysis algorithm, $(w/h)_{img} = 0.962$ and that obtained *via* the CW method, $(w/h)_{CW} =$
354   0.955. There is only a very small difference (less than 1%) between these two values.
355
356   3.2.3 Image Analysis of Treated Feathers
357
358   Figure 8 shows micrograph images (100×290 pixels) of duck feather samples
359   following treatment with detergent or magnetic particles along with the control
360   sample (no treatment). In each case the image on the left of each pair is the original
361   image and the image on the right of the pair is that which was obtained using the
362   image analysis algorithm following grey scale removal. These images clearly show
363   the extents of disruption to the grid patterns that have been imparted by the different
364   treatments where the treatment using magnetic particles seemingly imparts less
365   disruption to the grid pattern than that of the detergent treatment. It is important to
366   note however, that such disruption to the grid pattern following these different
367   treatments provides an indication of the feather condition at the time of treatment. It
368   does not necessarily indicate the condition of the feather in the longer term when, for
369   example, preening and the return of preening oils may improve feather condition.
370
371   >>>Insert Figure 8
372
373   The images shown in Figure 8 were further analysed using the software and the
374   respective area distribution histograms were produced (see Figure 9). The plots in
375   Figure 9 confirm quantitatively the observations that can be made by visual inspection
376   of Figure 8. The profiles of the control sample and the sample treated with magnetic
377   particles are similar and have w/h ratios of 0.561 and 0.600 respectively. This
378   represents a difference of *ca*. 7%. The w/h ratio for the detergent-treated sample is
379   significantly greater (0.743) than either of the latter (difference of *ca*. 20%).
380
381   >>>Insert Figure 9
382
383   The distribution histogram for the detergent treated sample exhibits a long "tail" that
384   corresponds to the larger open areas in its grid-like pattern. These are apparent in the
385   corresponding micrograph image and reflect the greater extent of disruption to the
386   grid pattern caused by the detergent treatment as compared with the magnetic particle
387   treatment (see Figure 8). A very strong correlation between the w/h ratio for feathers
388   treated with detergent and the concentration of detergent has also been shown to exist

389 (Orbell *et al*., 2007) in the case where the *w/h* ratio was determined manually using
390 the CW method.

391
392 **4. Conclusions**
393

394 The image analysis algorithm developed in this work provides a reliable quantitative
395 means of determining the coherency of a two-dimensional grid-like pattern that
396 reflects the feather microstructure of the Mallard Duck. The algorithm produces a
397 result that is consistent with theoretical computer-generated grids as well as with the
398 pattern observed in the micrographs of the feather microstructure. This analysis
399 technique successfully identified differences in the grid coherency of the feather
400 structure following different cleansing treatments and, as such, is proposed as a
401 possible quantitative indicator of the condition of this type of feather at the point in
402 time following the treatment. The effects of residual oil, metal, detergent or other
403 contaminants on the outcome produced by the technique has not been taken into
404 account and is yet to be explored.

405

406 Nonetheless, this work provides an important proof of principle, namely that such
407 indicators could be useful for the routine quantitative assessment of feather condition,
408 either for the trialling of different treatment protocols, as a tool during the
409 rehabilitation process, or as an assessment of feather condition in veterinary studies
410 along with other indicators, to give a more complete and objective assessment of
411 feather condition than is currently possible. Furthermore, it is suggested that the
412 method will be a valuable tool in helping to answer some remaining key questions
413 such as: how much if any, of the feather disruption is permanent and how much can
414 be reversed by preening and what is the impact of this disruption on a whole living
415 animal and its feathers in a variety of different environments and life stages. Work
416 along these lines is continuing in our laboratory.

417
418

425
426 **References**
427

428 Behnke, J., McGregor, P., Cameron, J., Hartley, I., Shepherd, M., Gilbert, F., Barnard, C., Hurst, J.,
429 Gray, S., Wiles, R., 1999. Semi-quantitative assessment of wing feather mite (*Acarina*) infestations on
430 passerine birds from Portugal. Journal of Zoology, 248(3), 337-347.

431
432 Bigger, S.W., Ngeh, L.N., Orbell, J.D., 2010. Mathematical model for the sequestering of chemical
433 contaminants by magnetic particles. Journal of Environmental Engineering, 136(11), 1255-1259.

434

435 Bigger, S.W., Munaweera, K., Ngeh, L.N., Dann, P., Orbell, J.D., 2013. Mathematical model for the
436 sequential pick-up of chemical contaminants by magnetic particles. Journal of Environmental
437 Engineering, 139(6), 796-802.

438

439 Carleton, R.E., Proctor, H.C., 2010. Feather mites associated with eastern bluebirds (*Sialia sialis L.*) in
440 Georgia, including the description of a new species of *Trouessartia* (*Analgoidea: Trouessartiidae*).
441 Southeastern Naturalist, 9(3), 605-623.

442

443 Cassie, A.B.D., Baxter, S., 1944. Wettability of porous surfaces. Transactions of the Faraday Society,
444 40**,** 546-541.

445

446 Department of Primary Industries (2012). Procedure – Oil/Chemical Spill Wildlife Response –
447 Rehabilitation of Wildlife. Biosecurity Operations Branch. Orange, New South Wales, Australia. 12
448 pp. [Available at: http://www.dpi.nsw.gov.au/__data/assets/pdf_file/0008/432098/Oil-Chemical-Spill-
449 Wildlife-Response-Rehabilitation-of-Wildlife-V1.pdf]
450 Elder, W.H., 1954. The oil glands of birds, The Wilson Bulletin, 66, 6-31.

451

452 Elowson, A.M., 1984. Spread-wing postures and the water repellency of feathers: A test of Rijke's
453 hypothesis, The Auk, 101(2), 371-383.

454

455 McLanaghan, K., Levy, S., 1996. CRC Standard Mathematical Tables and Formulae (D. Zwillinger,
456 Ed.) 30th edn., CRC Press, Boca Raton, Ch. 4, p. 270.

457

458 Murray, K.E., 1962. Studies in waxes. Australian Journal of Chemistry, 15(3), 510-520.

459

460 Ngeh, L.N., 2002. The development of magnetic particle technology for application to environmental
461 remediation. PhD Thesis, Victoria University, Australia, Ch. 5.

462

463 Ngeh, L.N., Orbell, J.D., Bigger, S.W., Munaweera, K., Dann, P., 2012. Magnetic cleansing for the

464 provision of a 'quick clean' to oiled wildlife. World Academy of Science, Engineering & Technology,

465 72, 1091-1093.

466 Odham, G., Stenhagen, E., 1971. On the chemistry of preen gland waxes of waterfowl. Accounts of
467 Chemical Research, 4(4), 121-128.

468

469 O'Hara, P.D., Morandin, L.A., 2010. Effects of sheens associated with offshore oil and gas
470 development on the feather microstructure of pelagic seabirds. Marine Pollution Bulletin, 60, 672-678.

471

472 Orbell, J.D., Godhino, L., Bigger, S.W., Nguyen, T.M., Ngeh, L.N., 1997. Oil spill remediation using
473 magnetic particles – An experiment in environmental technology. Journal of Chemical Education,
474 74(12), 1446-1448.

475

476 Orbell, J.D., Ngeh, L.N., Bigger, S.W., Zabinskas, M., Zheng, M., Healy, M., Jessop, R., Dann, P.,
477 2004. Whole-bird models for the magnetic cleansing of oiled feathers. Marine Pollution Bulletin, 48(3),
478 336-340.

479

480 Orbell, J.D., Dao, H.V., Ngeh, L.N., Bigger, S.W., 2007. Magnetic particle technology in
481 environmental remediation and wildlife rehabilitation. Environmentalist, 27, 175-192.

482

483 Rijke, A.M., 1968. The water repellency and feather structure of cormorants, *Phalacrocoracidae*.
484 Journal of Experimental Biology, 48(1), 185-189.

485

486 Rijke, A.M., 1970. Wettability and phylogenetic development of feather structure in water birds.
487 Journal of Experimental Biology, 52(2), 469-479.
488
489 Rijke, A.M., Jesser, W.A., Evans, S.W., Bouwman, H., 2000. Water repellency and feather structure of
490 the blue swallow *Hirundo atrocaerulea*. Ostrich, 71(1-2), 143-145.
491
492 Ryan., S., 2005. The development of a quantitative indicator of feather damage utilizing digital
493 imaging technology. MSc Thesis, Victoria University, Australia, Ch. 5.
494
495 Safarikova, M., Safarik, I., 2001. The application of magnetic techniques in biosciences. Magnetic and
496 electrical Separation, 10(4), 223–252.
497
498 Stephenson, R., 1997. Effects of oil and other surface-active organic pollutants on aquatic birds.
499 Environmental Conservation, 24(2), 121-129.
500
501 Stephenson, R., Andrews, C.A., 1997. The effect of water surface tension on feather wettability in
502 aquatic birds. Canadian Journal of Zoology, 75(2), 288-294.
503
504 Stettenheim, P.R., 1972. The Integument of Birds. In: Farmer, D.S., King, J.R. (Eds.) Avian Biology.
505 Academic Press, New York, Vol. 2, pp. 1-63.
506
507 Stocker, L., 2000. Practical Wildlife Care, Blackwell Science, London.
508
509 Zhao, Y., Yin, H., Dong, B., 2013. Use of infrared thermography to assess laying hen feather coverage.
510 Poultry Science, 92(2), 295-302.
511
512
513

Figure Captions

Fig 1. Two-dimensional grids generated by the Monte Carlo computer algorithm and that were randomly disrupted using disruption factors of: (i) $f = 0$, (ii) $f = 0.6$ and (iii) $f = 1.0$.

Fig 2. Selection of area distribution histograms for the quadrilaterals comprising computer-generated 20×20 grids subjected to different extents of random disruption as determined by the disruption parameter f where: $f = 0.3$ (filled circles), $f = 0.6$ (open circles) and $f = 0.9$ (filled squares).

Fig 3. Plot of the ratio w/h *versus* the disruption parameter f for a computer-generated grid where the grid component areas were calculated from equation (9). Calculation parameters: 20×20 grid; 100 iterations; 50 channels area resolution.

Fig 4. Selection of area distribution histograms for 20×20 grids produced by the grid generating algorithm and where the images were processed by the image analysis algorithm using 1 data averaging cycle. Disruption parameters: $f = 0.3$ (filled circles), $f = 0.6$ (open circles) and $f = 0.9$ (filled squares).

Fig 5. Plot of the ratio w/h *versus* the disruption parameter f for area distribution histogram data derived from computer-generated 20×20 grids where the images were processed by the image analysis algorithm using 1 data averaging cycle.

Fig 6. Plot of $(w/h)_{\text{img anal}}$ *versus* $(w/h)_{\text{calc}}$ where the corresponding ratios were determined for a series of computer-generated grids with the disruption parameter f varying between 0.1 and 1.0 at increments of 0.1.

Fig 7. Area distribution histograms of the grid-like pattern of a Mallard Duck feather micrograph where the distributions were independently determined using: (i) the image analysis algorithm (filled circles) and (ii) the CW method (open circles).

Fig 8. Micrograph images ($5\times$) of Mallard Duck feather samples following treatment with: (i) detergent and (ii) magnetic particles. The control sample (no treatment) is also shown. In each pair of images, the image on the left is the original and the one on the right is the corresponding image with its grey scale removed.

556   **Fig 9.** Area distribution histograms derived from the image analysis algorithm (5
557   data averaging cycles) for Mallard Duck feather samples (Figure 8) that were
558   subjected to: (i) detergent (filled squares) and (ii) magnetic particle (open
559   circles) treatment. The control sample (filled circles) is shown for
560   comparison.
561

562 **Figure 1**
563
564
565
566
567
568
569
570
571
572
573
574
575
576
577
578
579
580
581
582 **Figure 2**
583
584
585
586
587
588
589
590
591
592
593
594
595
596
597
598
599
600

601 **Figure 3**
602
603
604
605
606
607
608
609
610
611
612
613
614
615
616
617
618
619
620
621
622
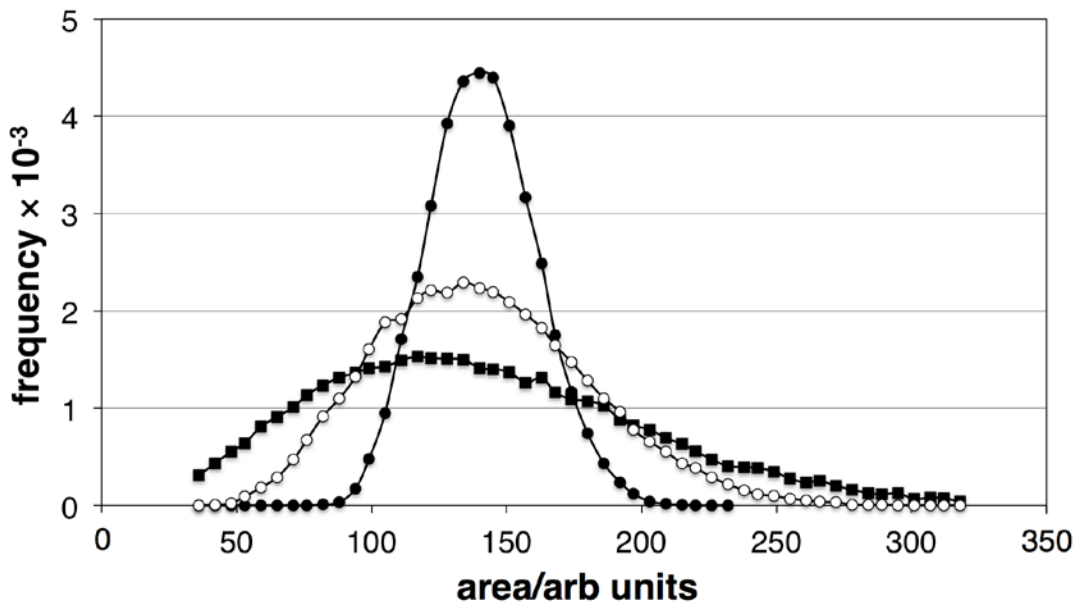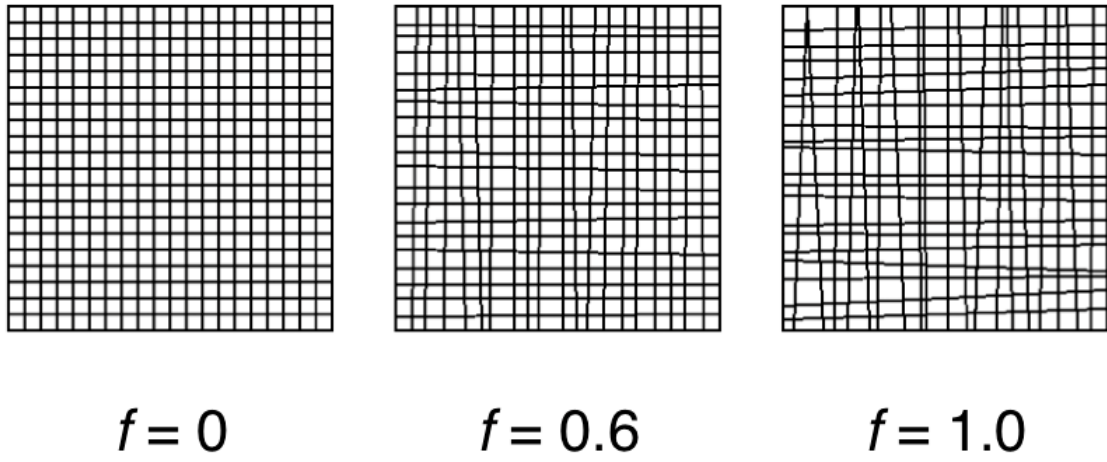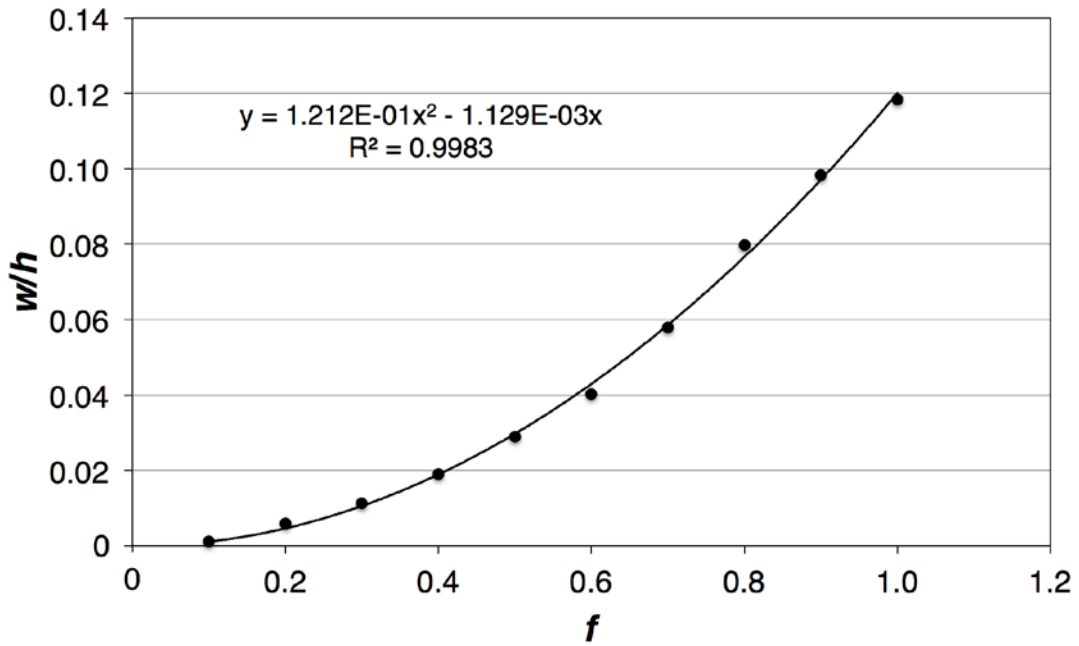
623 **Figure 4**
624
625
626
627
628
629
630
631
632
633
634
635
636
637
638
639
640
641
642
643
644
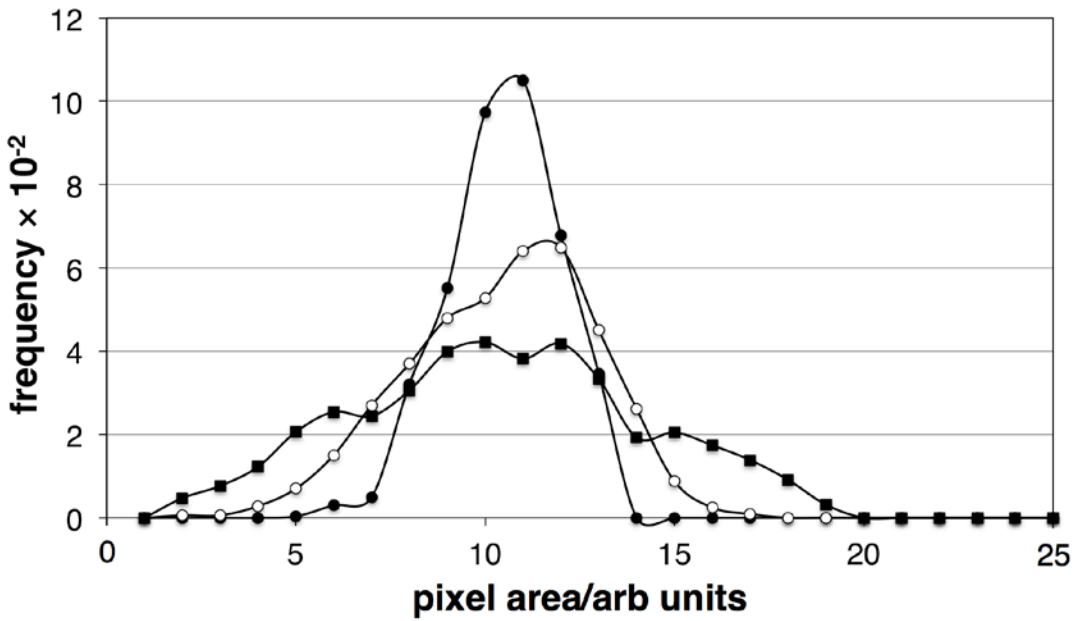
645 **Figure 5**
646
647
648

$y = 3.021E\text{-}02x^2 - 6.367E\text{-}04x$
$R^2 = 0.9436$

667 **Figure 6**
668
669

$y = 3.928E\text{+}00x + 7.823E\text{-}04$
$R^2 = 0.9362$

689 **Figure 7**

690
691
692
693
694
695
696
697
698
699
700
701
702
703
704
705
706
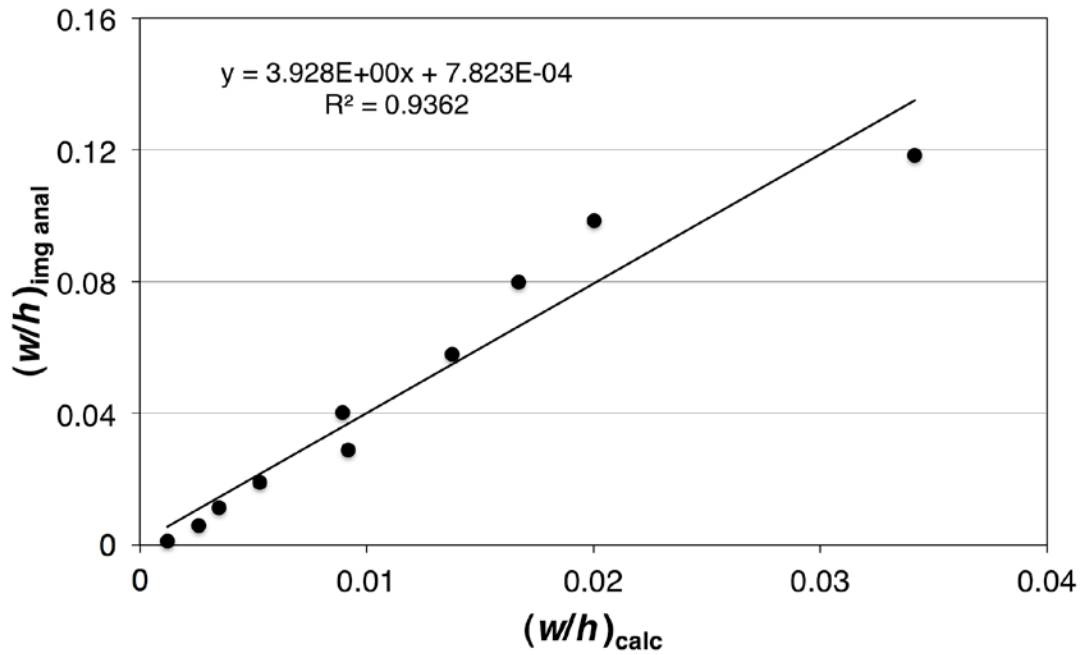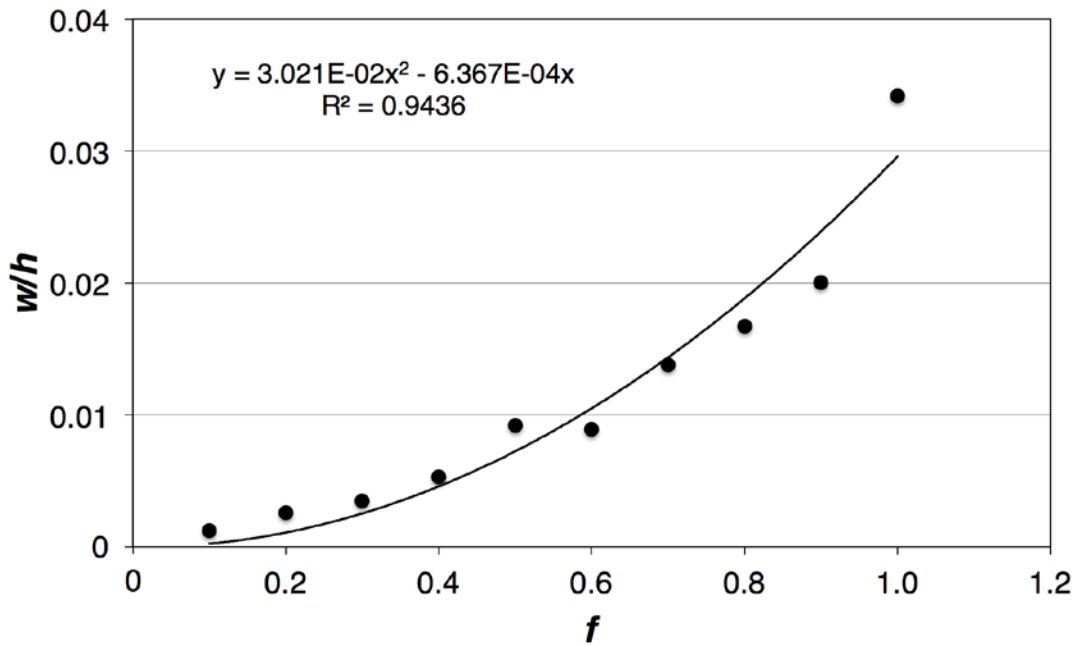
707
708
709
710
711 **Figure 8**

712
713
714
715
716
717
718

Control   Detergent treatment   Magnetic particle treatment

719
720
721
722
723
724
725
726
727
728

729
730
731
732
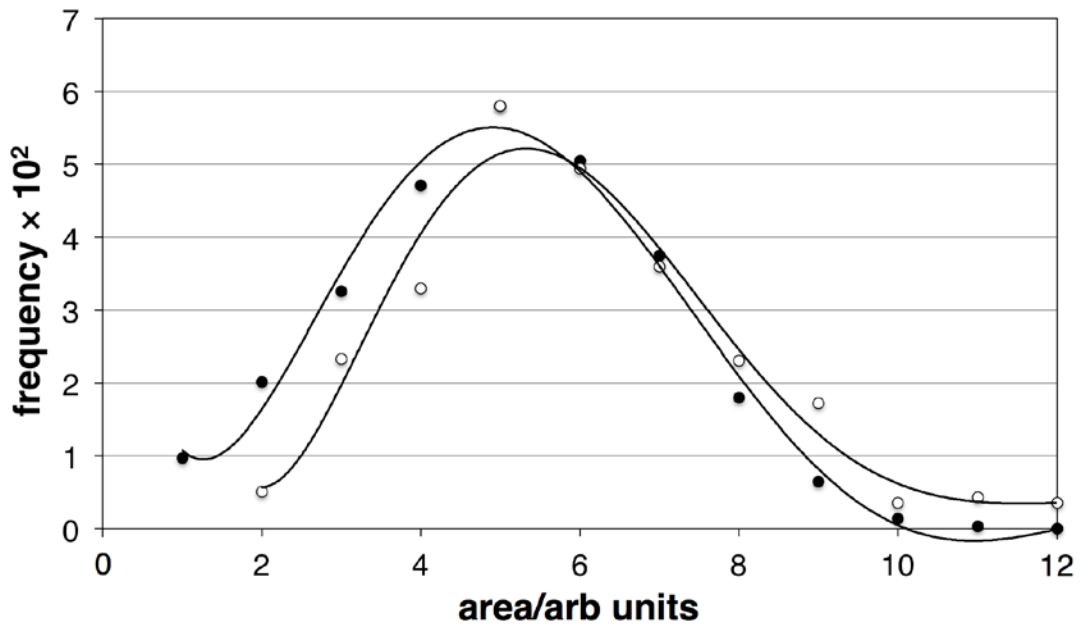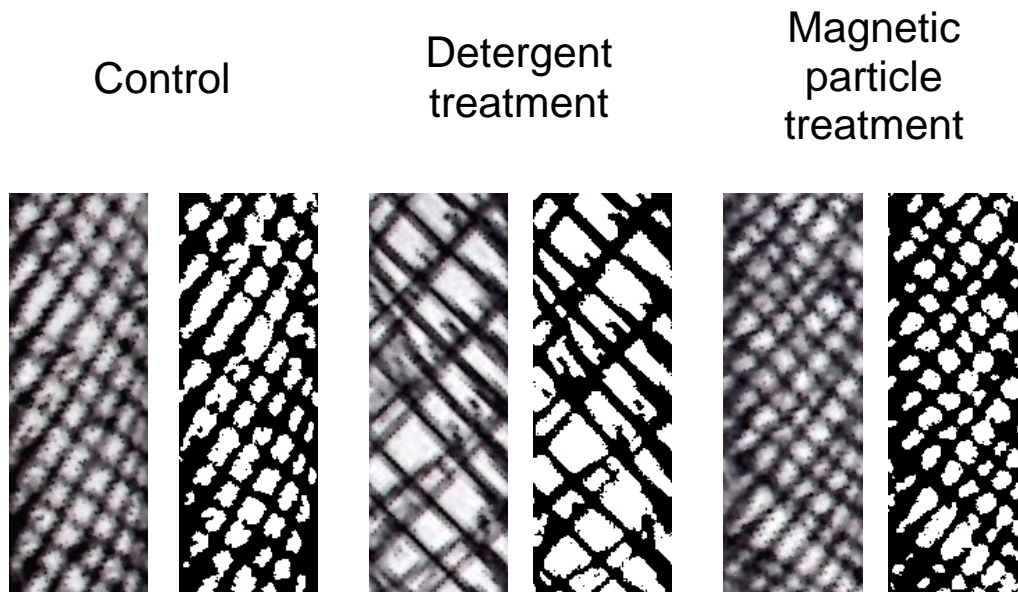
733   **Figure 9**

734

735

736

737

738

739

740

741